Journal of Theoretical and Applied Vibration and Acoustics 9(1) 61-72 (2023)

I S A V

Journal of Theoretical and Applied Vibration and Acoustics

journal homepage: http://tava.isav.ir

Investigation of similarity or dissimilarity in aerodynamic performance and noise pollution of H-Darrieus wind turbines

Mohamad Javad Zarei [a], **Alireza Bozorgi** [b,*]

[a] *M.Sc. Student, Department of Mechanical Engineering, University of Tehran, Tehran, Iran*

[b] *Assistant Professor, Department of Mechanical Engineering, Arak University of Technology, Arak, Iran*

ARTICLE INFO

Article history:
Received 30 April 2023

Received in revised form
22 June 2023

Accepted 29 August 2023

Available online 2 September 2023

Keywords:
VAWT

Noise pollution

Aeroacoustics

CFD

Aerodynamics

ABSTRACT

This article investigates the impact of wind speed on the non-dimensional curve of the power coefficient-tip speed ratio and noise pollution of an H-Darrieus wind turbine. The Unsteady Reynolds-Averaged Navier-Stokes (URANS) and the SST-kω turbulence model are applied to simulate flow around the turbine at four wind speeds and four tip speed ratios. The results show no similarity in the aerodynamic performance when wind speed changes. Additionally, noise pollution is investigated using the Ffowcs Williams-Hawkings (FW-H) equations at the tip speed ratio of 2.64 for all wind speeds. The directivity is calculated at distances of 4 m and 16 m and angle positions of 0^o to 360^o. It is observed that although the noise behavior is more similar to the monopole form, the angle position has a considerable effect on the noise received by observers. Increasing the wind speed significantly amplifies the wind turbine noise, but there is no similarity in the directivity profiles obtained for all wind speeds. Finally, the frequency distribution is investigated, and the results show that the highest frequency is at blade passing frequency in all cases. However, the results based on rotor frequencies show no similarity in the shape of frequency distribution.

© 2023 Iranian Society of Acoustics and Vibration, All rights reserved.

1. Introduction

Renewable energy is a rapidly expanding industry that is significantly important in the fight against climate change. The world's renewable energy capacity has increased considerably, with nearly

* Corresponding author:
E-mail address: a.bozorgi@ut.ac.ir (A. Bozorgi)

http://dx.doi.org/10.22064/tava.2023.2001020.1224

295 GW added in 2022 alone (a 9.57 % increase compared to 2021), owing mainly to the growth of solar and wind power [1]. Wind power accounts for nearly 26.6% of global renewable capacity in 2022 [1]. Looking into the future, it is clear that wind power will continue to play a significant role in the worldwide energy supply. Research by the International Renewable Energy Agency (IREA) shows that it is necessary to increase the wind energy capacity by 335 GW annually until 2050 to limit the increase in global temperature to 1.5 degrees [2]. Because of the growing importance of wind turbines, their issues have become one of the most popular topics in engineering and energy. Wind turbines are split into vertical axis and horizontal axis groups. Vertical axis wind turbines (VAWTs) have grown in popularity in urban and suburban settings in recent years. They can produce electricity from the wind blowing from any direction, making them more versatile and simpler to incorporate into existing structures. Moreover, their compact size and design make them a suitable option for residential and commercial buildings where space is limited.

However, one of the drawbacks of VAWTs is the noise they generate during operation. As wind turbines become more common in urban environments, the issue of noise pollution is becoming increasingly important. Several researches show that the noise of wind turbines can cause annoyance, sleep disruption, and psychological distress in people who live near wind turbines [3-6]. Furthermore, studies have shown that the heart rates of wind turbine workers can change when exposed to noise levels of 85 decibels or higher [7-10]. Considering these findings, extensive research on wind turbine noise is critical, particularly for VAWTs located near residential areas. VAWT noise is classified as mechanical and aerodynamic. While mechanical noise can be reduced using current manufacturing techniques, aerodynamic noise remains a significant issue for these turbines.

Many studies have been conducted on the aerodynamic performance of these turbines. Mohammad et al. [11] investigated the effect of changing the pitch angle on the output power of an H-Darrieus turbine. Their research used a two-dimensional flow simulation, revealing that zero degree was the most effective angle for this turbine. Omgad et al. [12] optimized the wind lens geometry using three-dimensional flow simulation and achieved an 82% increase in the output power of an H-Darrieus turbine with a tip speed ratio of 2.75. However, their analysis revealed that using a wind lens increased the noise level of the turbine. Hashem and Mohamed [13] investigated 24 airfoil types from various families in a three-bladed turbine at tip speed ratios ranging from 2 to 7 and determined the best airfoil from each family. Mohammad et al. [14] also investigated 25 symmetrical and asymmetrical airfoils. The profile of LS(1)-0413 airfoil was introduced as the optimal geometry. Singh et al. [15] used a two-dimensional simulation to assess the starting moment of a three-blade turbine at various rigidities (ranging from 0.8 to 1.2) by changing the rotor diameter. The findings revealed that decreasing the rotor diameter improves the self-starting performance. Click et al. [16] also used two-dimensional simulations to investigate how changing the number of blades affects the starting moment. Their studies involved turbines with 2 to 5 blades, and the results showed that increasing the number of blades improves the turbine's self-starting performance.

Mohamed [17] explored the impact of blade shape on the noise of an H-Darrieus wind turbine using four different airfoils (NACA63418, S1046, FXLV152, and NACA0018). It was found that the S1046 airfoil generates lower noise than the other shapes. In addition, Mohamed [17] studied the effect of solidity on noise by varying rotor radius and discovered that increased solidity led to

more noise. Using the FW-H equations, Ghasemian and Nejat [18] calculated the noise produced by a three-bladed turbine with NACA4518 geometry at different speed ratios and distances from the turbine. Jio et al. [19] investigated the effect of working speed on the noise produced by a three-bladed H-Darrieus turbine with NACA0021 geometry at various tip speed ratios and distances. They found that higher speeds increased noise production due to turbulence.

2. Governing equations

This study applied the two-dimensional form of continuity and URANS equations to simulate the flow around an H-Darrieus wind turbine. The governing equations for the Cartesian coordinates are given as follows:

$$\frac{\partial \rho}{\partial t} + \frac{\partial}{\partial x_j}(\rho u_j) = 0 \tag{1}$$

$$\frac{\partial}{\partial t}(\rho u_i) + \frac{\partial}{\partial x_j}(\rho u_i u_j) = -\frac{\partial p}{\partial x_i} + \frac{\partial}{\partial x_j}\left(\mu\left(\frac{\partial u_i}{\partial x_j} + \frac{\partial u_j}{\partial x_i} - \frac{2\delta_{ij}}{3}\frac{\partial u_i}{\partial x_i}\right)\right) + \frac{\partial}{\partial x_j}(\tau_{ij}) \tag{2}$$

where ρ is the density, u is the velocity component, i and j are directions, p is the pressure, μ is the dynamic viscosity, τ_{ij} is the Reynolds stress tensor term, and δ_{ij} is the Kronecker delta. The SST-kω turbulence model [20, 21] was employed to capture turbulence effects in the flow simulation accurately. This model considers both the turbulent kinetic energy k and the specific dissipation rate (ω). The SST-kω model offers distinct advantages for simulating complex flows, such as those encountered in wind turbines. This model combines the strengths of the k-ε and k-ω models and is widely used for simulating turbulent flows in various fields, such as H-Darrieus wind turbines. For example, Rezaei et al. [22] investigated different turbulence models for the two-dimensional solution of H-Darrieus turbines and concluded that SST models, including SST-kω, SSTI and TSST exhibit the most reasonable agreement with experimental results.

The FW-H equations [23] , as a rearrangement of Navier-Stokes equations, are widely used for calculating the noise generated by moving bodies. The FW-H equation by defining blade walls as data surface (where f = 0) is given by

$$\left\{\frac{1}{{c_0}^2}\frac{\partial^2}{\partial t^2} - \frac{\partial^2}{\partial {x_i}^2}\right\}[p'(\boldsymbol{x},t)H(f)] = \frac{\partial}{\partial t}[Q\delta(f)] - \frac{\partial}{\partial x_i}[L_i\delta(f)] + \frac{\partial^2}{\partial x_i \partial x_j}[T_{ij}H(f)] \tag{3}$$

In where,

$$\begin{aligned} &Q = \rho_0 v_n;\ \ L_i = P_{ij}n_j \\ &T_{ij} = \rho u_i u_j + \left(p - p_0 - {c_0}^2(\rho - \rho_0)\right)\delta_{ij} - \sigma_{ij} \end{aligned} \tag{4}$$

Equations (3) and (4) include various parameters to calculate the noise propagated from the rotor. Sound speed is represented by c_0, and noise sources are categorized into monopole sources Q, dipole sources L_i, and quadrupole sources T_{ij}. v_n presents the normal component of data surface velocity, P_{ij} the compressive stress tensor, σ_{ij} the viscous stress tensor, and n_j the normal unit vector of data surface. Mean values are represented by 0. The monopole and dipole sources are defined only on the data surface because of the Dirac delta function δ(f). On the other hand, the quadrupole sources are defined outside the data surface because of the step function H(f). The

monopole and dipole sources, defined on the blade surface, are used to calculate the noise propagated from the rotor.

3. Numerical simulation

ANSYS Fluent software was used to simulate the flow domain of a three-bladed H-Darrieus turbine. The geometric parameters and airflow characteristics are shown in Table 1. Two dimensionless parameters of λ and Cp were used for validation, and are given by

$$\lambda = \frac{R\omega}{U_\infty} \tag{5}$$

$$C_p = \frac{T\omega}{0.5\rho U_\infty^3 A} \tag{6}$$

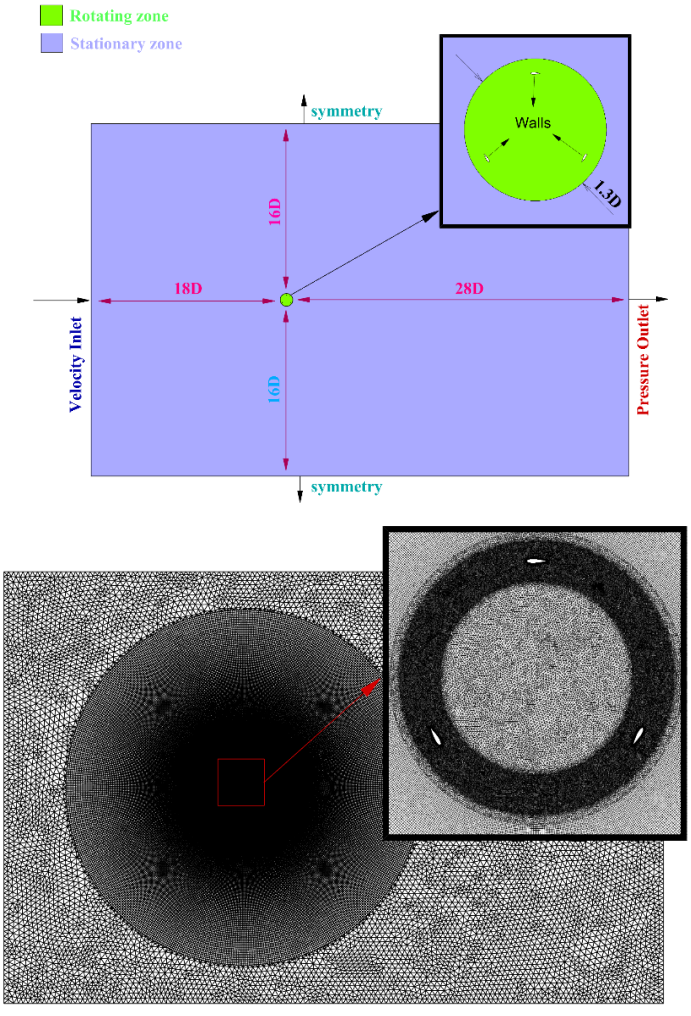

Fig. 1: Flow domain and boundary conditions

where λ and C_p are the tip speed ratio and power coefficient, respectively. R is rotor radius, ω is rotational speed, T is shaft torque, ρ is density, and A is the swept area. Figure 1 depicts the flow simulation domain and boundary conditions. A mesh independence study was performed on several meshes ranging from 120,000 to 780,000 cells to ensure the accuracy and reliability of the simulation results. The study showed that the relative deviation in the C_p calculation was less than 1% for the case with more than 232,658 cells. Therefore, a mesh with 381,324 cells was selected for all simulations. In this mesh, the average orthogonal quality on the stationary and rotating zones was 0.995 and 0.943, respectively. The equiangular skewness on the stationary and rotating zones was 0.014 and 0. 162, respectively. After careful consideration, a mesh with 380,000 cells was chosen. As depicted in Figure 2, the flow domain was meshed using boundary layer mesh in such a way that the average of Y^+ on the blade wall is 1.5. Rosario et al. [24] investigated different pressure-velocity coupling methods and discovered that the SIMPLE algorithm is the most suitable approach in VAWT simulations, so the SIMPLE algorithm was used. The second-order upwind method was used for turbulence and momentum discretization, the second-order method for the pressure term, and the second-order implicit method for time discretization. A comparison of the CFD results to experimental data and other numerical simulations is shown in Figure 3, which suggests the reliability of the results.

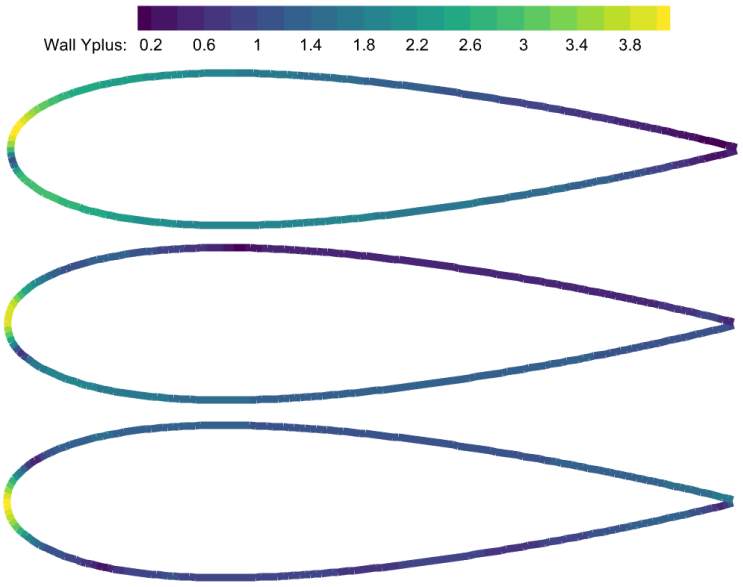

Fig. 2: Y^+ on Blades in λ=2.51

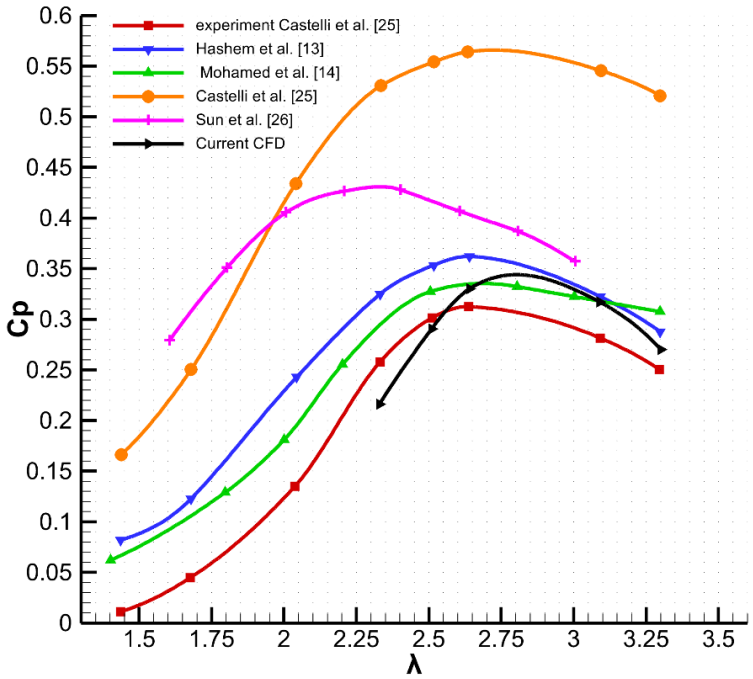

Fig. 3: Validation of the CFD results

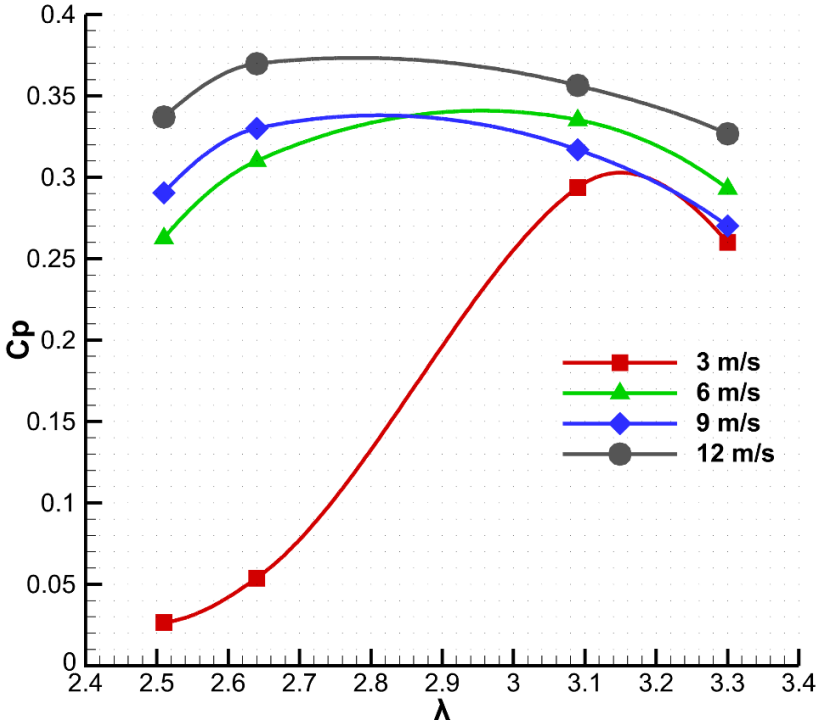

Fig. 4: Cp-λ curve for different wind speeds

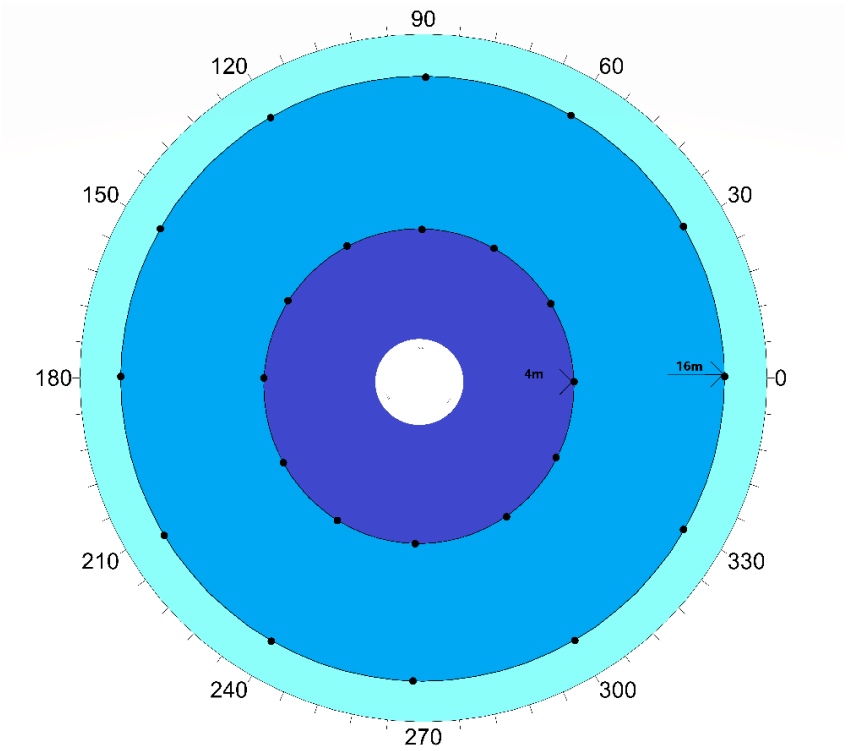

Fig. 5: The position of observers

4. Results

This section investigates how changes in wind speed affect Cp-λ curves and noise pollution. The simulation was performed at wind speeds of 3, 6, 9, and 12 m/s, and the rotating speed was changed to achieve λ values of 2.51, 2.64, 3.09, and 3.3 for each wind speed. Figure 4 shows a considerable difference between dimensionless Cp-λ curves when wind speed changes. For example, at λ = 2.51, the value of Cp at 12 m/s wind speed is 12.66541353 times greater than at 3 m/s wind speed. This extreme deviation means the similarity cannot be used for the dimensionless Cp-λ curve. It can be because of a change in Reynolds number. For an identical λ, the ratio of wind speed is equal to the ratio of Reynolds number, e.g., increasing the wind speed from 3 m/s to 12 m/s quadruples the Reynolds number.

Moreover, it was observed that the wind speed can have an opposite effect on the Cp. For example, an increase in wind speed from 6 m/s to 9 m/s amplifies the Cp in the λ of 2.51 and 2.64 but weakens the Cp in the λ of 3.09 and 3.3. The highest Cp is for the wind speed of 12 m/s and the lowest for the wind speed of 3 m/s in all values of λ.

Directivity diagrams were prepared at radial distances of 4 and 16 m from the rotor center at a speed ratio of 2.64 (figure 6) to investigate the impact of observer distance on the received noise. The Sound Pressure Level (SPL) in dB is calculated as follows:

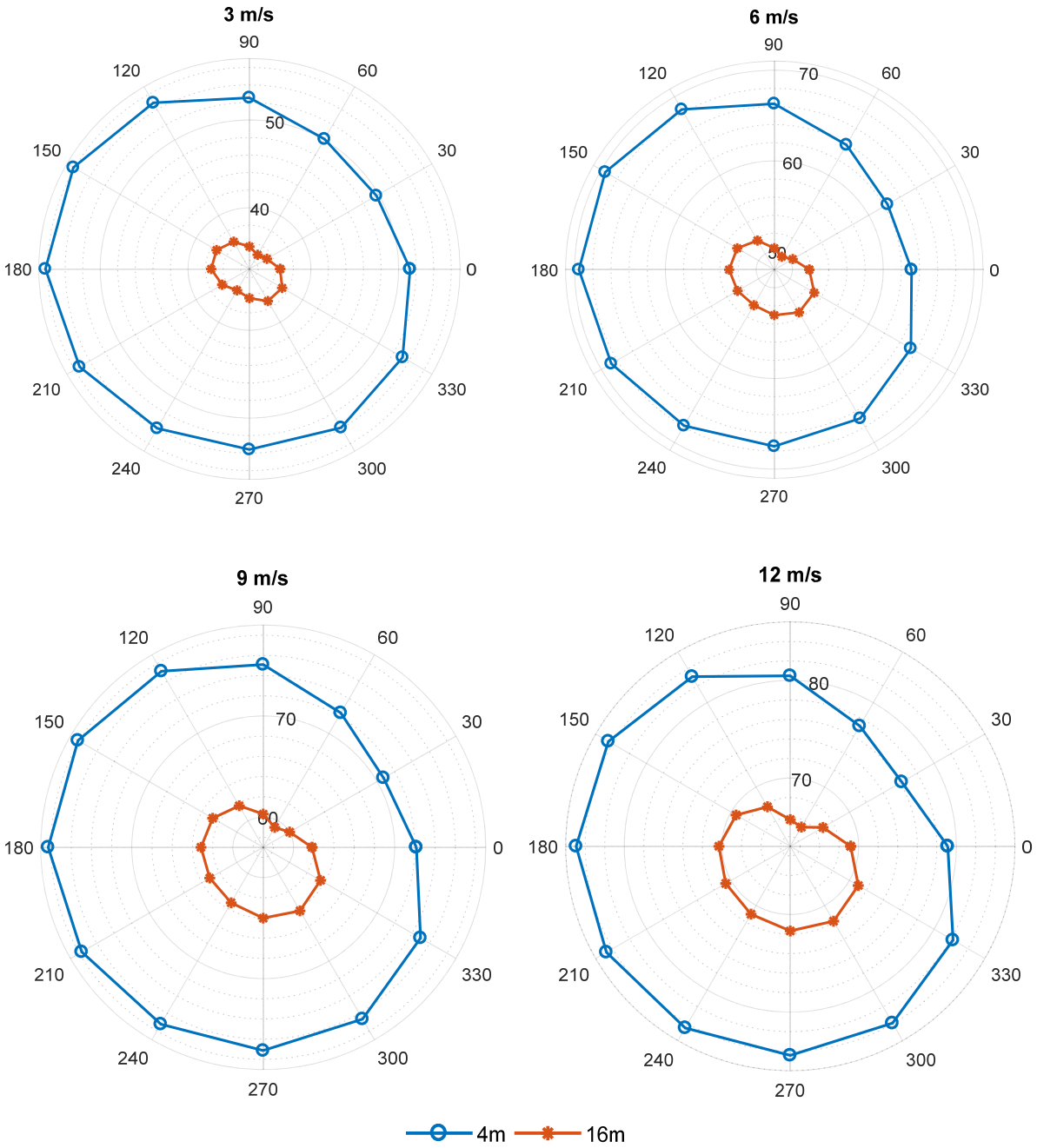

Fig. 6: Directivity for different wind speeds

$$SPL = 20log\frac{p}{p_{ref}} \tag{7}$$

where P_{ref} is reference sound pressure with the value of 2×10^{-5} Pa.

Figure 6 demonstrates that the noise received by the observers varies with angle position. It is because of aerodynamic asymmetry conditions around the rotor, which increases the need to calculate noise in all directions around the rotor. However, the results show that the noise behavior resembles the monopole form.

It should be noted that dB is a logarithmic scale, and every 3 dB of noise reduction equals halving the root mean square of acoustic pressure. It is observed that the effect of change in observer distance is not identical for different angle positions. For example, Figure 6a (3 m/s wind speed) shows that the movement of observers from 4 m to 16 m decreases the SPL to 14.30 and 18.96 dB at angle positions of 30° and 180°, respectively. As a result, the graph of 3 m/s wind speed has the most noise reduction (Figure 6a), and the graph of 12 m/s wind speed has the least noise reduction due to the increase in the distance.

For more investigations, the noise pollution for identical distances is shown in Figure 7. It is observed that the increase in wind speed causes an increase in noise. This diagram shows that changing the flow velocity will not affect the noise propagation at different angles. Moreover, there is no similarity in the directivity profile for various wind speeds.

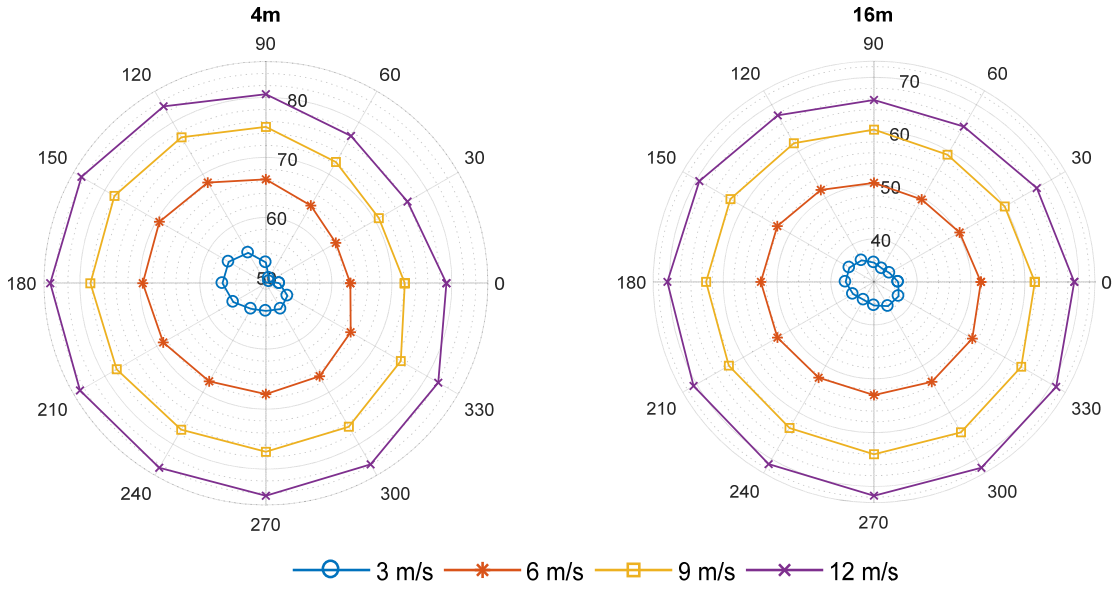

Fig. 7: Comparing the directivity in identical distances

For an identical tip speed ratio, the increase ratio in wind speeds is equal to the increase ratio in rotational speeds. Therefore, the frequency distribution changes when wind speed changes. Figures 8 and 9 describe the frequency distribution at the tip speed ratio of 2.64 and four angle positions of the observers (30°, 120°, 210°, and 300°). The frequency distribution has been calculated using Fast Fourier Transform (FFT). The results show that in all wind speeds, the

highest peak is located at Blade Passing Frequency (BPF), equal to three times the rotor frequency ($BPF = \text{blade numbers} \times \frac{\omega(\text{rad/s})}{2\pi} = 3\frac{\omega(\text{rad/s})}{2\pi} = 3f_{rotor}$).

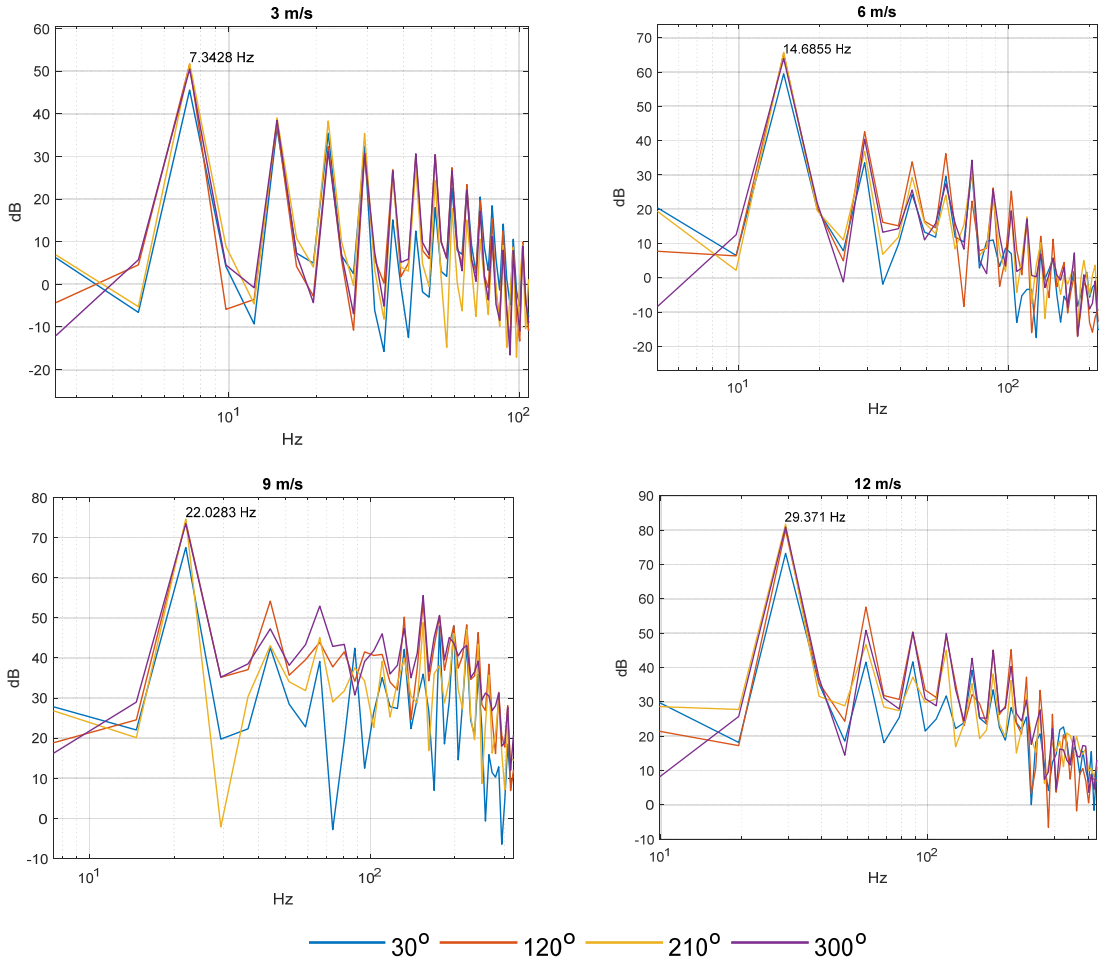

Fig. 8: Frequency distribution for R= 4 m

Figure 10 shows the frequency distribution based on the rotor frequency to investigate the similarity in frequency distribution. The results show no similarity in the shape of the frequency distribution.

5. Conclusion

This study investigated the similarity or dissimilarity in the aerodynamic performance and noise pollution of an H-Darrieus Wind Turbine by changing the wind speed. At first, the flow around the blades was simulated and validated using the URANS and SST-kω turbulence model. Then, the non-dimensional Cp-λ curve was extracted for four wind speeds of 3, 6, 9, and 12 m/s in four tip speed ratios of 2.51, 2.64, 3.09, and 3.3. The results showed no similarity in the aerodynamic performance because of a considerable difference between the values of Cp-λ curves, such that even the shape of the curves was not similar. It was observed that an increase in wind speed could

have opposite effects on Cp. The increase in some cases amplifies Cp while, in some cases, weakens Cp.

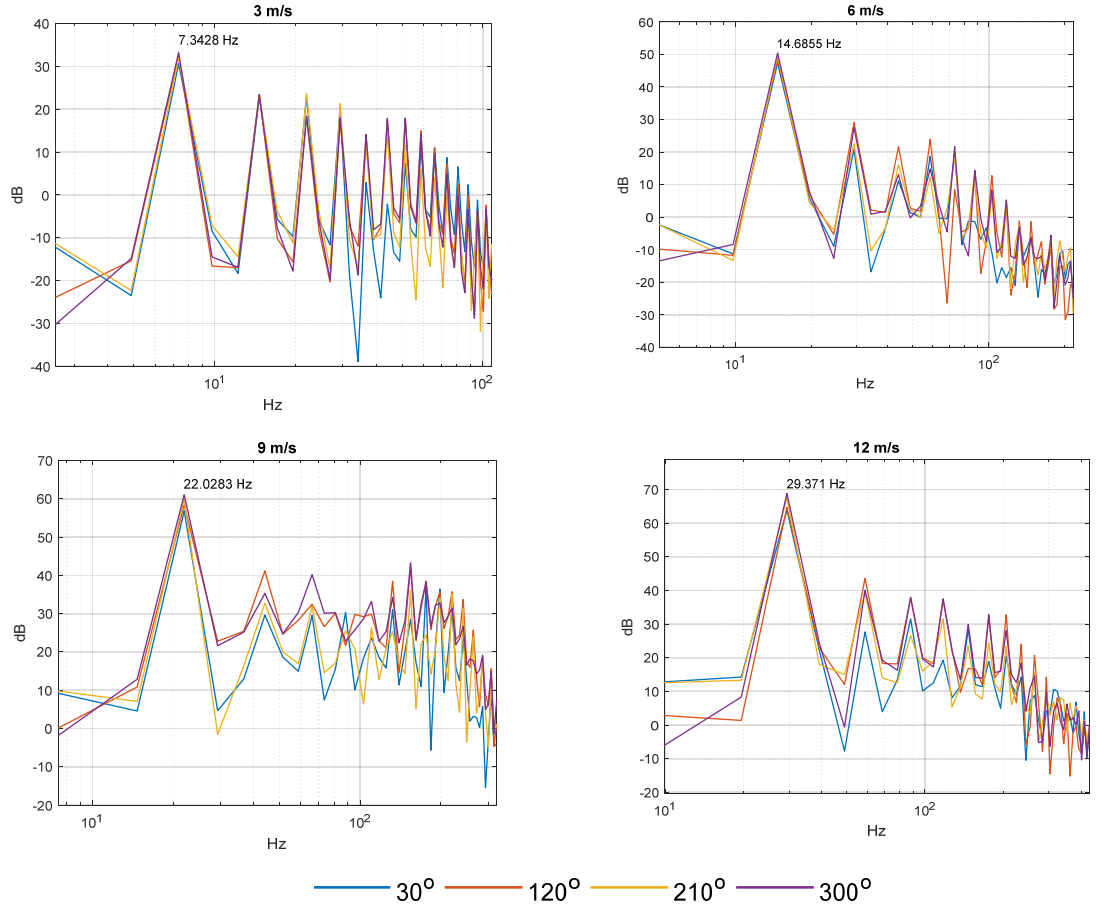

Fig. 9: Frequency distribution for R= 16 m

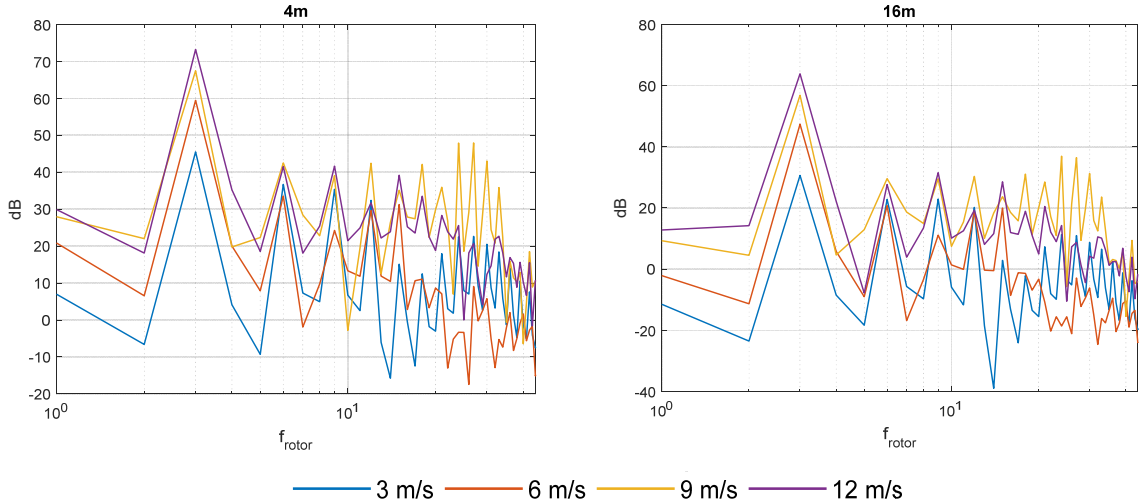

Fig. 10: Frequency distribution based on rotor frequencies (θ = 30°)

Additionally, noise pollution was investigated using the FW-H equations at $\lambda = 2.64$ for the different wind speeds. The noise was calculated at distances of 4 and 16 m and angle positions of 0° to 360°. It was observed that the angle position considerably affects the noise received by observers. Moreover, the results showed that the noise behavior resembled the monopole form. By increasing the wind speed, noise pollution of the wind turbine increased at all points, but there is no similarity in the shape of the profiles. Finally, the frequency distribution was investigated using FFT. In all cases, the highest frequency was located at the BPF, but the results based on rotor frequencies showed no similarity in the shape of frequency distribution.

References

[1] E. Asmelash, R. Gorini, International oil companies and the energy transition, International Renewable Energy Agency, Abu Dhabi, 2021.
[2] IRENA, World energy transitions outlook: 1.5° C pathway, International Renewable Energy Agency, Abu Dhabi, 2021.
[3] K.P. Waye, E. Öhrström, Psycho-acoustic characters of relevance for annoyance of wind turbine noise, Journal of sound and vibration, 250 (2002) 65-73.
[4] R.H. Bakker, E. Pedersen, G.P. van den Berg, R.E. Stewart, W. Lok, J. Bouma, Impact of wind turbine sound on annoyance, self-reported sleep disturbance and psychological distress, Science of the total environment, 425 (2012) 42-51.
[5] T. Van Renterghem, A. Bockstael, V. De Weirt, D. Botteldooren, Annoyance, detection and recognition of wind turbine noise, Science of the Total Environment, 456 (2013) 333-345.
[6] A. Smith, A review of the non-auditory effects of noise on health, Work & stress, 5 (1991) 49-62.
[7] C. Clark, K. Paunovic, WHO environmental noise guidelines for the European region: a systematic review on environmental noise and quality of life, wellbeing and mental health, International journal of environmental research and public health, 15 (2018) 2400.
[8] E.E. Van Kempen, H. Kruize, H.C. Boshuizen, C.B. Ameling, B.A. Staatsen, A.E. De Hollander, The association between noise exposure and blood pressure and ischemic heart disease: a meta-analysis, Environmental health perspectives, 110 (2002) 307-317.
[9] T.-Y. Chang, R.-M. Jain, C.-S. Wang, C.-C. Chan, Effects of occupational noise exposure on blood pressure, Journal of occupational and environmental medicine, 45 (2003) 1289-1296.
[10] S. PorAbdian, M. Ghotbi, H.A. Yousefi, E. Habibi, M. Zare, The epidemiologic study on hearing standard threshold shift using audiometric data and noise level among workers of Isfehan metal industry, Koomesh, 10 (2009) 253-260.
[11] M. Mohamed, A. Ali, A. Hafiz, CFD analysis for H-rotor Darrieus turbine as a low speed wind energy converter, Engineering Science and Technology, an International Journal, 18 (2015) 1-13.
[12] A. Dessoky, G. Bangga, T. Lutz, E. Krämer, Aerodynamic and aeroacoustic performance assessment of H-rotor darrieus VAWT equipped with wind-lens technology, Energy, 175 (2019) 76-97.
[13] I. Hashem, M. Mohamed, Aerodynamic performance enhancements of H-rotor Darrieus wind turbine, Energy, 142 (2018) 531-545.

[14] M. Mohamed, A. Dessoky, F. Alqurashi, Blade shape effect on the behavior of the H-rotor Darrieus wind turbine: Performance investigation and force analysis, Energy, 179 (2019) 1217-1234.
[15] M. Singh, A. Biswas, R. Misra, Investigation of self-starting and high rotor solidity on the performance of a three S1210 blade H-type Darrieus rotor, Renewable Energy, 76 (2015) 381-387.
[16] Y. Celik, L. Ma, D. Ingham, M. Pourkashanian, Aerodynamic investigation of the start-up process of H-type vertical axis wind turbines using CFD, Journal of Wind Engineering and Industrial Aerodynamics, 204 (2020) 104252.
[17] M. Mohamed, Aero-acoustics noise evaluation of H-rotor Darrieus wind turbines, Energy, 65 (2014) 596-604.
[18] M. Ghasemian, A. Nejat, Aero-acoustics prediction of a vertical axis wind turbine using Large Eddy Simulation and acoustic analogy, Energy, 88 (2015) 711-717.
[19] J. Su, H. Lei, D. Zhou, Z. Han, Y. Bao, H. Zhu, L. Zhou, Aerodynamic noise assessment for a vertical axis wind turbine using Improved Delayed Detached Eddy Simulation, Renewable energy, 141 (2019) 559-569.
[20] F.R. Menter, Two-equation eddy-viscosity turbulence models for engineering applications, AIAA journal, 32 (1994) 1598-1605.
[21] F.R. Menter, Review of the shear-stress transport turbulence model experience from an industrial perspective, International journal of computational fluid dynamics, 23 (2009) 305-316.
[22] A. Rezaeiha, H. Montazeri, B. Blocken, On the accuracy of turbulence models for CFD simulations of vertical axis wind turbines, Energy, 180 (2019) 838-857.
[23] J.F. Williams, D.L. Hawkings, Sound generation by turbulence and surfaces in arbitrary motion, Philosophical Transactions for the Royal Society of London. Series A, Mathematical and Physical Sciences, (1969) 321-342.
[24] R. Lanzafame, S. Mauro, M. Messina, 2D CFD modeling of H-Darrieus wind turbines using a transition turbulence model, Energy Procedia, 45 (2014) 131-140.